crystals

MDPI

Article

Microstructure, Dielectric Properties and Bond Characteristics of Lithium Aluminosilicate Glass-Ceramics with Various Li/Na Molar Ratio

Minghan Li [1,2], Lingqi Kong [3], Wenzhi Wang [1,2], Yanping Ma [1,2,*] and Hong Jiang [1,2,*]

[1] State Key Laboratory of Marine Resources Utilization in South China Sea & Special Glass Key Lab of Hainan Province, Hainan University, Haikou 570228, China; 19080500110006@hainanu.edu.cn (M.L.); 20085600210057@hainanu.edu.cn (W.W.)
[2] Collaborative Innovation Center of Marine Science and Technology, Hainan University, Haikou 570228, China
[3] School of Physics and Optoelectronic Engineering, Hainan University, Haikou 570228, China; 20213006427@hainanu.edu.cn
* Correspondence: myp@hainanu.edu.cn (Y.M.); 184444@hainanu.edu.cn (H.J.); Tel.: +86-13178932567 (Y.M.); +86-18876901999 (H.J.)

Abstract: The advent of 5G technology presented new challenges regarding the high-frequency characteristics of electrical signals and their impact on the cover glass properties of electronic devices. This study aimed to analyze the effect of the Li/Na molar ratio on the dielectric and mechanical properties, as well as the structural characteristics, of lithium aluminosilicate glass-ceramics. Using the melting method, we prepared lithium aluminosilicate base glasses and subsequently crystallized them by adjusting the molar ratio. XRD and TEM analyses were employed to investigate the resultant structures and crystal formation in the five base glasses. It was observed that $Li_2Si_2O_5$ and $LiAlSi_4O_{10}$ crystals precipitated, exhibiting varying degrees of crystallinity and crystal ratios. Through a comparison of dielectric properties before and after crystallization, it was found that the dielectric constants of the glass-ceramics were consistently reduced. This decrease can be attributed to the lower dielectric constants exhibited by both crystalline phases compared to the parent lithium aluminosilicate glasses. Furthermore, the presence of glass crystals effectively immobilized the alkali metal ions within the glass phase, impeding their movement under an electric field. Consequently, the dielectric loss value of the glass-ceramics decreased with the increasing amount of precipitated crystals. By carefully adjusting the composition and optimizing the crystallization process, we successfully produced lithium aluminosilicate glass-ceramics, demonstrating excellent mechanical and optical properties, coupled with low dielectric properties.

Keywords: glass-ceramics; crystalline grain; mechanical properties; dielectric loss

Citation: Li, M.; Kong, L.; Wang, W.; Ma, Y.; Jiang, H. Microstructure, Dielectric Properties and Bond Characteristics of Lithium Aluminosilicate Glass-Ceramics with Various Li/Na Molar Ratio. *Crystals* **2023**, *13*, 1647. https://doi.org/10.3390/cryst13121647

Academic Editor: Tomasz Sadowski

Received: 29 October 2023
Revised: 23 November 2023
Accepted: 24 November 2023
Published: 29 November 2023

1. Introduction

The world has now embraced the 5G era, with 5G signals being characterized by millimeter waves. These waves possess high frequencies (ranging from 0.45 to 6 GHz) and short wavelengths. However, it is worth noting that the materials utilized in mobile phones and other electronic devices can impact the efficiency of 5G signal transmission due to their dielectric loss properties. Consequently, in order to optimize the transmission efficiency and minimize such losses, extensive research has been conducted on the high-frequency dielectric properties of different materials. Among these materials, glass-ceramics have garnered significant attention as they are extensively used in electronic equipment.

Glass-ceramics are a composite material of ceramic phases and glass, crystallized via a glass-melting process and temperature control [1]. In comparison to pure ceramics, glass-ceramics exhibit a remarkable reduction in pore volume. Furthermore, the dielectric constant of glass-ceramics is no longer primarily influenced by the amount of pores but, rather, by numerous factors, including the type of crystal phase, degree of crystallinity,

grain size, and composition of the residual glass phase [2–4]. When glass-ceramics possess a high degree of crystallinity, the dielectric constant is primarily determined by the major crystalline phase. Nevertheless, in cases where the degree of crystallinity is low, the presence of the residual glass phase can lead to a significant increase in dielectric loss. Consequently, enhancing the crystallinity of the glass system during the heat treatment process is of paramount importance. Previous studies have indicated that the addition of oxides as sintering additives or nucleating agents into the glass matrix can enhance the crystallinity of the glass and facilitate densification [5–7].

Lithium aluminosilicate glass-ceramics (Li_2O-Al_2O_3-SiO_2, LAS) find widespread use in the electronic industry due to their exceptional mechanical and optical properties, low thermal expansion coefficient, minimal dielectric loss, and excellent thermal stability [8–10]. As a result, numerous researchers have focused on studying the influence of base-glass composition and crystal phase types on the dielectric properties of lithium aluminosilicate glass-ceramics. For instance, Guanyu Chen et al. fabricated glass-ceramics using β-spodumene as the primary crystal phase, which exhibited a dielectric constant of 5.8 and a dielectric loss of 1.3×10^{-3} at a test frequency of 10 MHz [11]. Zhenjun Qing's team prepared LAS glass-ceramics through a sintering method and discovered that the dielectric properties were influenced by the material's structure. The inclusion of pores in the glass-ceramics resulted in a reduction in dielectric constant and an increase in dielectric loss. In their study, the sample containing 3 wt% B_2O_3 demonstrated optimal dielectric properties, with a dielectric constant of 7.2 and a dielectric loss of 1.4×10^{-3} (test condition: 1 MHz) [12]. Krasnikov et al. investigated the impact of Mg^{2+} and Ba^{2+} ions on the dielectric properties of lithium aluminosilicate glass-ceramics and found that the addition of Ba^{2+} ions led to a lower dielectric constant [13]. Another study conducted by Hamidreza Savabieh et al. focused on adjusting the crystallization process of LAS glass to obtain a hexagonal spodumene crystal phase. The increase in crystallization temperature allowed for the observation of the phase transition from hexagonal spodumene to tetragonal rutile, which, in turn, affected the dielectric properties. The dielectric constant decreased from 7.5 to 6.6, and the dielectric loss increased to 0.081 during the precipitation of the hexagonal spodumene phase. Subsequently, during the phase transition from hexagonal to tetragonal, the dielectric loss reduced to 0.052. Additional densification at higher temperatures did not impact the loss value, thus maintaining a constant value (the test condition was 100 Hz to 2 MHz) [14].

In order to achieve broader applications of glass-ceramics, in addition to dielectric properties, people also focus on their mechanical and optical characteristics. For example, Zhiqiang Zhou and Feng He et al. [15] studied the effect of Na_2O content on the crystallization of lithium aluminosilicate glass-ceramics, and they prepared glass-ceramics with a low expansion coefficient and excellent mechanical properties. Jiang Shi and Feng He et al. [16] explored the effect of the Na_2O/BaO ratio on crystallization by changing the ratio in the Li_2O-Al_2O_3-$B2O_3$-SiO_2 low-temperature glass-ceramics and found that $BaAl_2Si_2O_8$ crystals are the main factor affecting the mechanical properties of glass-ceramics. Wentao Zhang et al. [17] studied the effect of Al/Na variation on Q^n (the number of (SiO_4) units with bridging oxygen atoms) and explored the process system for preparing glass-ceramics with excellent mechanical properties through orthogonal experiments. Weichang Li et al. [18] prepared glass-ceramics with lithium disilicate ($Li_2Si_2O_5$) as the main crystalline phase, and the addition of fluorine increased the crystallinity and promoted the formation of $Li_2Si_2O_5$ crystals, thereby enhancing the mechanical properties. Chenjie Ji et al. [19] prepared transparent glass-ceramics with eucryptite and nepheline crystalline phases as the main crystalline phases, achieving high levels of microhardness, elastic modulus, and fracture toughness.

So far, many teams have been devoted to the study of lithium aluminosilicate glass-ceramics and have successfully identified the basic glass composition, common phases such as β-quartz solid solution and β-spodumene, as well as the effect of crystallinity on the dielectric properties of lithium aluminosilicate glass-ceramics. Considering practical usage scenarios, their mechanical and optical properties should also be equally emphasized.

Currently, comprehensive studies on the mechanical, optical, and dielectric properties of lithium aluminosilicate glass-ceramics are still relatively scarce. Therefore, our team delved deeply into the effects of compositional changes on the structure and properties of lithium aluminosilicate glass-ceramics. In order to obtain uniform bulk basic glass, we chose the melting method. At the same time, we adjusted the Li/Na molar ratio in the lithium aluminosilicate base glass to study its microstructure, as well as its dielectric, mechanical, and optical properties.

2. Experiments

2.1. Preparation of Glass-Ceramics

SiO_2, H_3BO_3, and $NH4H_2PO_4$ (purity: 98%; XiLONG SCIENTIFIC, Shantou, China), Li_2CO_3, Na_2CO_3, and Al_2O_3 (purity: 99%; Macklin, Shanghai, China), and ZrO_2 (purity: 99%; Alladdin, Shanghai, China) were transferred to a quartz crucible, fully blended for 20 min using an automated mixer, then heated to 1100 °C for 30 min in a high-temperature furnace. The combination was then entirely melted by gradually heating the glasses to 1520 °C at a rate of 10 °C/min. The glasses were kept at 1520 °C for two hours in order to retain uniformity and clarity. After being poured into a mold, the hot glasses quickly cooled to solidify into a block. To lessen internal stress, the block was cooled to 25 to 30 °C after being annealed for four hours at 450 °C in a muffle furnace. The mold was warmed to 200 °C. The composition of lithium aluminosilicate glass-ceramics is shown in Table 1.

Table 1. Composition design of Li_2O-Al_2O_3-SiO_2 system glass-ceramics (wt%).

Formulation (wt.%)	SiO_2	Al_2O_3	Li_2O	Na_2O	B_2O_3	P_2O_5	ZrO_2
T1	68.86	3.71	21.62	0.86	2.15	0.93	1.86
T2	68.86	3.71	20.62	1.86	2.15	0.93	1.86
T3	68.86	3.71	19.62	2.86	2.15	0.93	1.86
T4	68.86	3.71	18.62	3.86	2.15	0.93	1.86
T5	68.86	3.71	17.62	4.86	2.15	0.93	1.86

2.2. Structure Test

Differential scanning calorimetry was used to ascertain the crystals' non-isothermal kinetic characteristics (DSC). About 30 mg of fine glass powder with particle diameters between 1 and 10 μm was subjected to DSC examination using a NETZSCH STA 449 F5 thermal analyzer (Selb, Germany). A quartz crucible was filled with the powder, and the temperature was raised at a rate of 10 °C/min.

The glass-ceramics were crushed into a 200-mesh powder, and the powdered samples were examined for physical phases in the 10~80° temperature range using an X-ray diffractometer (SmartLab (3 kW), Rigaku, Tokyo, Japan). The Cu K radiation used in the X-ray diffractometer is 40 kV and 40 mA, and it was filtered using a graphite monochromator (=0.154 nm). The divergence, reception, and scattering slits were set at 1°, 0.15 mm, and 1°, respectively. The scanning speed was set to 10°/min. With the use of the MDI Jade 6.5 software, the relative composition of the crystalline phases was determined. The degree of crystallinity was then estimated using the results.

Using an XPM-Φ120×3 three-head grinder (Weiming Machinery Company, Ganzhou, China), the glass-ceramics were pulverized into a 200-mesh powder after undergoing the heat treatment process. The examination of powder sample phases was conducted utilizing an Thermo Nicolet iS50 Fourier transform infrared (FT-IR) spectrometer (Waltham, MA, USA). The examination was conducted at a temperature of 24 °C, encompassing a wavelength spectrum spanning from 0 to 1500 nm.

The surface morphology of the lithium aluminosilicate glass-ceramics samples was examined via scanning electron microscopy (SEM; TEScould MIRA3, Brno, Czech Republic) after they were etched with 5% hydrofluoric acid for 50 s, rinsed with deionized water, dried, and sputtered with gold dust. The acceleration voltage was adjusted to 10 kV during the analysis.

After ball milling, the glass-ceramics powder samples were put into acetone solvent, dispersed by ultrasonication for 15~20 min, and the dispersed liquid was dripped onto the carbon-copper grid and dried for 10 min. Bright-field TEM images, HR-TEM, and SAED patterns of the nanocrystalline grains in glass-ceramics were observed using Thermoscientific Talos F200 × 2 transmission electron microscope (Waltham, MA, USA).

2.3. Performance Test

Five kinds of lithium aluminosilicate base-glasses with different Li/Na molar ratios were cut into 4 × 4 × 1 mm pieces (two pieces for each kind), and one piece was taken out for crystallization. The dielectric constant and dielectric loss of base-glass and corresponding glass-ceramics were measured by Broadband dielectric impedance spectrometer (Novocontrol CONCEPT 80, Cologne, Germany), and the test frequencies were 0.5 GHz, 1 GHz, 1.5 GHz, 2 GHz, 2.5 GHz, and 3 GHz, respectively. The test temperature was 24 °C.

The 3-point bending method was utilized to conduct the bending strength test. The glass-ceramics were sliced into strips measuring 2 × 5 × 40 mm^3 and meticulously polished. The Yuhan Model YC-128A (Shanghai, China) universal mechanical testing machine was utilized to conduct bending strength testing, wherein the sample was subjected to pressure until the occurrence of a fracture. The sample size of the glass-ceramic was used, and the experimental span was set to 25 mm. The loading speed was 9.8 ± 0.1 Ns^{-1}. To ensure the accuracy of the experiment, avoid mechanical errors, and determine the standard deviation of the data, 20 tests were conducted on each sample. The Taiming HXD-1000TMC/LCD (Shanghai, China) microhardness tester was used to measure the hardness of the crystallized 10 × 10 × 1 mm^3 glass piece at 5 points, with an experimental loading time of 10 s and a loading pressure of 1.96 N. Subsequently, the 5 Vickers hardness values were averaged.

The PerkinElmer Lambda 650 (Waltham, MA, USA) ultraviolet–visible spectrophotometer was employed to evaluate the rate of visible light transmission in glass-ceramics. After being finely polished, the crystallized glass pieces, measuring 10 × 10 × 1 mm^3, were subjected to testing within the wavelength range of 380~800 nm.

3. Results and Discussion

3.1. DSC

The base-glasses for the lithium aluminosilicate system are depicted in Figure 1 through a DSC diagram. Table 2 displays the temperature points of the DSC curves, which are the glass transition temperature (T_g) and the first and second crystallization peaks (T_{m1} and T_{m2}, respectively). The glass transition temperature of all samples, as shown in Figure 1, is between 480 and 515 °C. At this temperature, the glass begins to significantly transform, and nucleation takes place. All samples' crystallization peak temperatures are also examined, and it is revealed that T_{m1} and T_{m2} are in the ranges of 650~680 °C and 720~775 °C, respectively. Fine grains begin to form in the glass at these temperatures.

Table 2. DSC curves of the lithium aluminosilicate glasses (°C).

Recipes	T1	T2	T3	T4	T5
T_g	480	490	495	505	515
T_{x1}	605	625	640	645	648
T_{p1}	650	670	675	680	685
T_{x2}	690	710	705	735	745
T_{p2}	720	750	735	765	775

Preliminary research suggests that when nucleation and crystallization heat treatments are conducted at a lower temperature, the glass-ceramics' interior has a propensity to precipitate minuscule nanosized and evenly distributed crystal particles [20]. By examining the DSC curves, it can be inferred that glass-ceramics can be produced in two stages. The foundation glass was heated to 570 °C (10 °C/min) for 1 h prior to use. The temperature was increased to 660 °C to allow for crystallization after the glass had nucleated. The

crystallization process was finished, and then the furnace was slowly cooled down to ambient temperature. Table 2 shows thermal parameters from the DSC study.

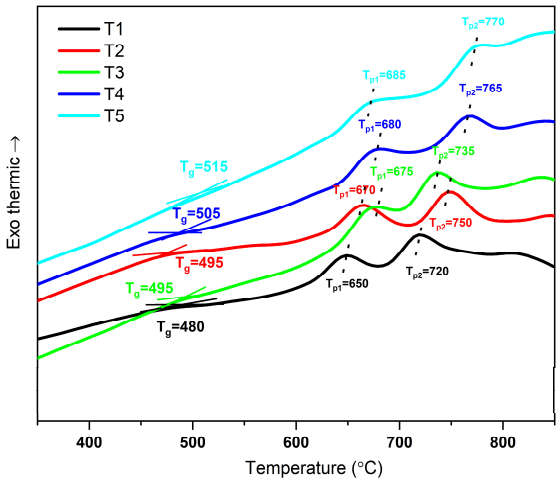

Figure 1. DSC curve of lithium aluminosilicate glasses.

3.2. Infrared (IR) Spectrum Analysis

Observation of the infrared spectra of lithium aluminosilicate glasses T1~T5 reveals three main absorption peaks in Figure 2, located near 470 cm^{-1}, 780 cm^{-1}, and 1053 cm^{-1}. The vibration peak at 470 cm^{-1} represents the Si-O bending vibration in the glass network structure [21,22], and the position of this absorption peak hardly changes with the variation in the Li_2O/Na_2O ratio in the glass composition. The absorption peak appearing at approximately 780 cm^{-1} may be related to the symmetric stretching vibration of Si-O-Si [22], and the position of this absorption peak shifts slightly as the Li_2O/Na_2O ratio decreases, moving from 785 cm^{-1} to 795 cm^{-1}, indicating the strengthening of Si-O-Si vibration in the network structure. All five samples' spectra exhibit an overlapping peak located at 900~1200 cm^{-1}, with its peak value at 1053 cm^{-1}, corresponding to the anti-symmetric stretching vibration of the (SiO_4) Q^3 unit. When the total number of lithium and sodium ions remains constant but Li^+ decreases and Na^+ increases, the vibration peak shifts towards lower wavenumbers [22,23], indicating a reduction in Q^3 units. The decrease in the number of Q^3 structural units in the network signifies a tendency towards loosening of the glass network structure, which is related to the disaggregation ability of different alkali metal ions.

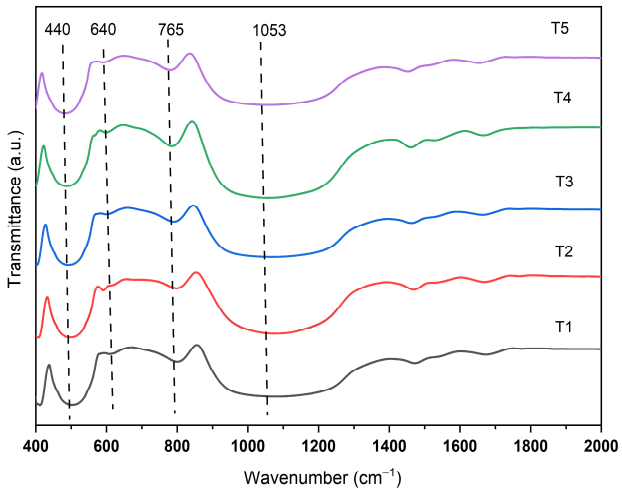

Figure 2. FT-IR spectrum of lithium aluminosilicate glass with different Li_2O/Na_2O molar ratios.

The infrared spectrum of T1~T5 lithium aluminosilicate glass-ceramics is depicted in Figure 3. It is evident that the absorption peak bands of the T1~T5 samples are largely consistent, with clear absorption bands near 440 cm^{-1}, 555 cm^{-1}, and 765 cm^{-1}, and the most prominent absorption bands are in the 900~1200 cm^{-1} range, with peaks at 1020 and 1078 cm^{-1}. The absorption bands at 440 cm^{-1} and 765 cm^{-1} exhibit a tendency to shift towards the lower-wavelength number band. The vibrational bands vary in both intensity and width, resulting in the sharpening of the vibrational peaks [24,25]. At the same time, the glass-ceramics strip is divided, resulting in two vibrational peaks at 555 cm^{-1} and 1020 cm^{-1}. The in-plane bending vibration of Si-O-Al in the glass network structure is responsible for the vibrational peak at approximately 555 cm^{-1}, whereas the asymmetric stretching vibration of Si-O-Al in the glass network structure is responsible for the vibrational peak near 1020 cm^{-1} [26,27]. The typical configuration of (SiO_4) in the lattice amplifies the intermolecular vibrations, causing the energy range (765 cm^{-1}) to move to the lower wave number range and divide the energy range. Due to the crystal's highly symmetrical structure, the vibrational bands become sharper and more powerful as a result of the narrower bond length and bond angle distributions [28–30]. With an increase in Na_2O content (T1~T5), there is a propensity for the vibrational peaks near 440 cm^{-1} and 765 cm^{-1} to transition from higher to lower wave numbers. This is consistent with the prevailing pattern of the base-glass, and both can be attributed to the disturbance of the glass network structure. The vibrational peaks at 1020 cm^{-1} expand and become more prominent as the amount of crystals deposited in the glass rises with the Li_2O concentration, thus intensifying the vibrational peaks connected to the crystals.

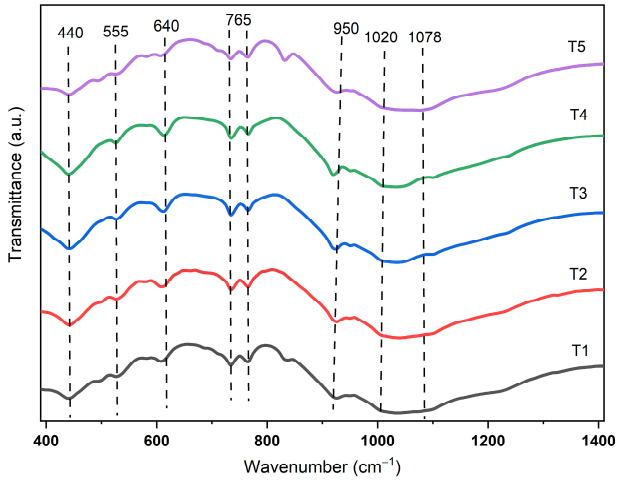

Figure 3. FT-IR spectrum of lithium aluminosilicate glass-ceramics with different Li_2O/Na_2O molar ratios.

Furthermore, all shelf silicate minerals exhibit certain bands of moderate intensity ranging from 550 to 850 cm^{-1}, which can be attributed to their polymeric structure. Within this range, Si-O-Al bending vibrations (560 cm^{-1}) and Al-O-Si symmetric stretching vibrations (640 cm^{-1}) can be observed [31]. It shows that Al atoms have entered the (SiO_4) tetrahedron, which partially replaced Si atoms in the tetrahedron, and some even completely replaced them, resulting in the formation of the (AlO_4) tetrahedron. At this time, (AlO_4) tetrahedron will have an extra negative charge. In order to keep the balance of electricity price, "Li^+" is filled near "Al^{3+}" to neutralize the electricity.

3.3. XRD

The XRD patterns of lithium aluminosilicate glass-ceramics (T1~T5) with different Li/Na molar ratios are shown in Figure 4. The main crystalline phases of T1~T5 glass-ceramics are all composed of $Li_2Si_2O_5$ (JCPDS #40–0376) and $LiAlSi_4O_{10}$ (JCPDS #35–0463) [32], but

their proportions are different. The ratio of $Li_2Si_2O_5$ to $LiAlSi_4O_{10}$ in five samples is shown in Table 3. According to the XRD pattern, the crystallinity of five glass-ceramics samples is over 70%. Among them, the crystallinity of the T2 sample is the highest, exceeding 90%. By examining Figures 5a and 6a, it is evident that the dielectric constants of the five samples diminished as the precipitation of $Li_2Si_2O_5$ and $LiAlSi_4O_{10}$ crystals precipitated, when comparing T1~T5 base-glass with the corresponding glass-ceramics. It is evident that the dielectric constant of the glass-ceramics sample is greater than the range of 1~3 GHz when the electric field frequency is 0.5~1 GHz. The high-frequency electric field causes the ion polarization frequency to be slower than the electric field frequency, resulting in the dielectric constant of the glass decreasing as the frequency increases. The dielectric constant of the crystallized sample, following heat treatment, is evidently inferior to that of the base-glass due to the lower dielectric constants of $Li_2Si_2O_5$ and $LiAlSi_4O_{10}$ in comparison to the lithium aluminum silicon base-glass containing a substantial quantity of Na^+ and Li^+. In accordance with the law of mixture, the dielectric constant of glass-ceramics can be calculated by adding together the products of dielectric constants from different phases and their respective volume fractions. When the Li/Na ratio of lithium aluminosilicate base-glass is changed, the volume fraction of the precipitated microcrystalline phase changes, and then the dielectric constant of glass-ceramics decreases as the crystallinity increases [33].

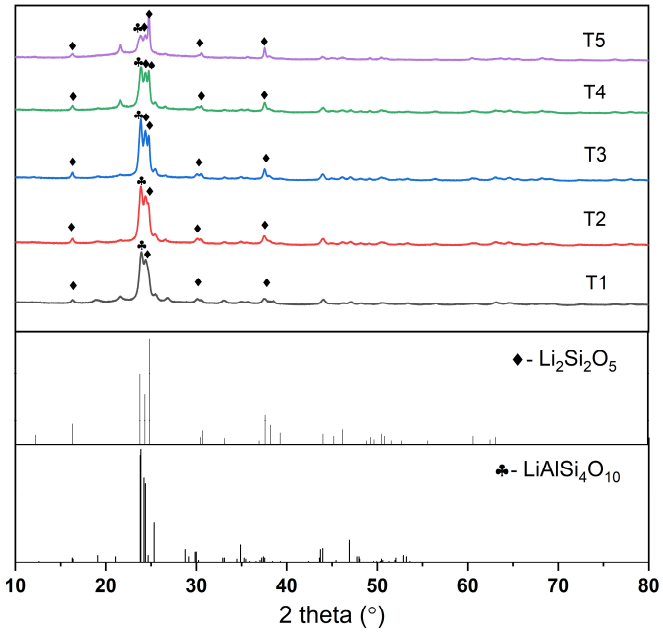

Figure 4. XRD pattern of T1~T5 lithium aluminosilicate glass-ceramics.

Table 3. Crystallinity of T1~T5 glass-ceramics and the ratio of two main crystal phases.

Sample	$Li_2Si_2O_5$ (%)	$LiAlSi_4O_{10}$ (%)	Crystallinity
T1	81.7	18.1	85.1%
T2	80.1	19.6	91.5%
T3	82.6	16.9	78.2%
T4	84.7	15.1	73.8%
T5	87.5	12.2	70.9%

Generally, the dielectric loss of the glass phase in glass-ceramics is higher than that of the precipitated crystal phase, which is the main factor causing dielectric loss [34]. Observing Figure 6b, it can be seen that the dielectric loss of the glass-ceramics treated by high-temperature crystallization is obviously lower than that of the glass sample, which

may be because the crystal phase precipitated in the glass solidifies the alkali metal ions and reduces their movement under the electric field [13], thus reducing the dielectric loss.

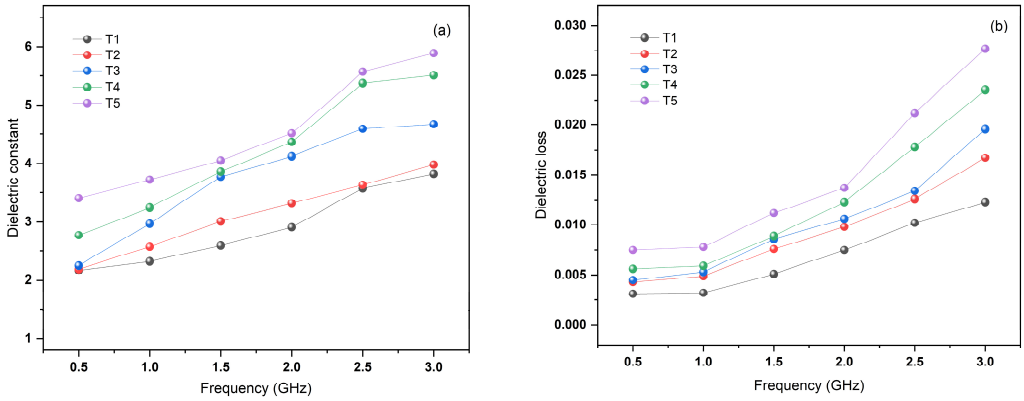

Figure 5. (**a**,**b**) dielectric constant and loss of T1~T5 lithium aluminosilicate glass samples.

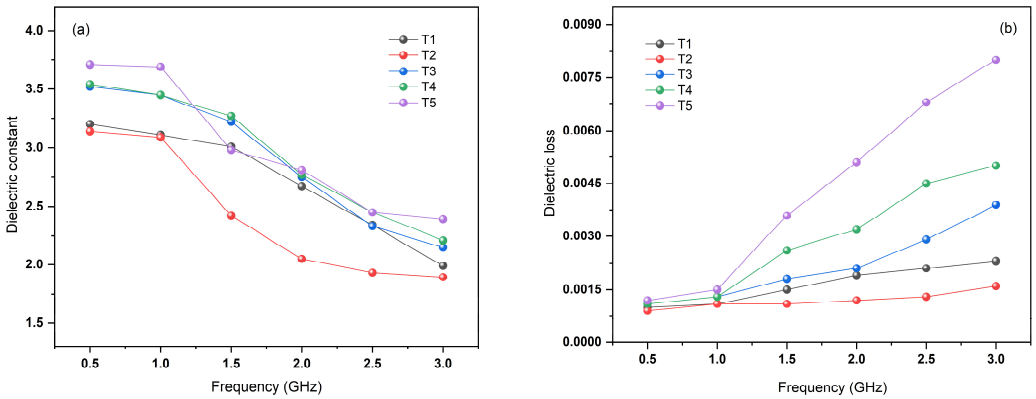

Figure 6. (**a**,**b**) dielectric constant and loss of T1~T5 lithium aluminosilicate glass-ceramics.

3.4. TEM

The microstructure of the T1~T5 glass-ceramics samples was examined using a transmission electron microscope. Bright-field TEM was utilized to examine the microstructure of glass-ceramics following heat treatment. The presence of two nanostalline phases was verified through SAED and high-resolution HR-TEM analysis [35]. The bright-field TEM, SAED, and HR-TEM images are depicted in Figure 7. Figure 7a represents a TEM image of a crystal bright field, while Figure 7b showcases the HR–TEM images of crystals, which correspond to the two crystals in the XRD spectrum. Additionally, Figure 7a allows for the observation of spherical nanocrystalline particles with an average size ranging from 100 to 200 nm. The SAED patterns of the glass-ceramics samples are shown in Figure 7c,d; there are two kinds of diffraction fringes, and their existence indicates that two kinds of crystals exist in the glass-ceramics. The lattice fringe spacing of the HR–TEM image shown in Figure 7(b-1) is 3.60 Å, which is close to the (111) crystal plane spacing of the $Li_2Si_2O_5$ crystal of 3.58 Å; the lattice stripe spacing in Figure 7(b-2) is 3.75 Å, which is very close to the (210) crystal plane spacing of the $LiAlSi_4O_{10}$ crystal. The results of electron diffraction are consistent with those of XRD.

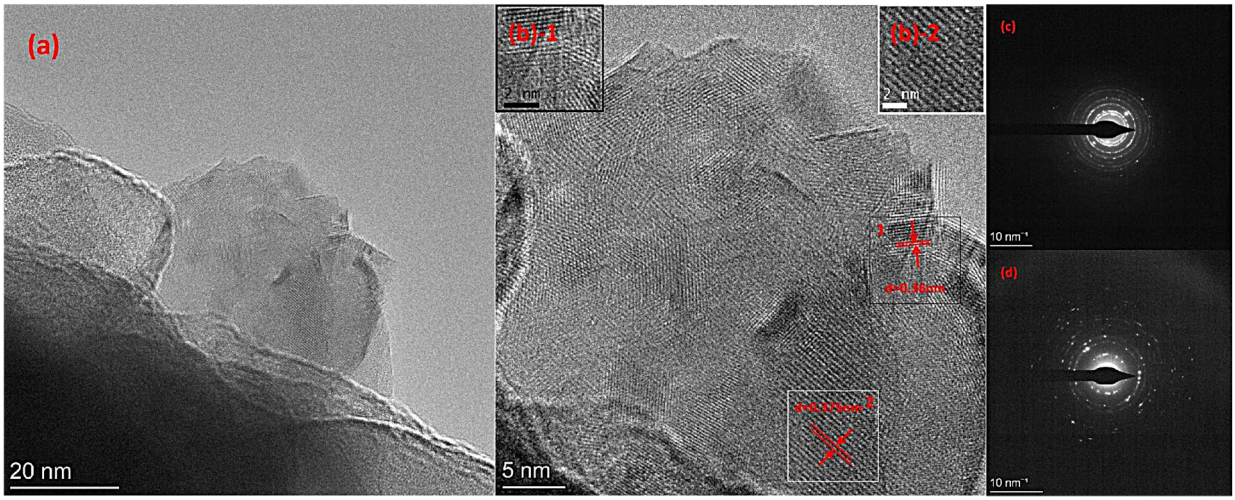

Figure 7. (**a**): Bright-field TEM images; (**c**,**d**): SAED patterns of $Li_2Si_2O_5$ and $LiAlSi_4O_{10}$ crystal; (**b**): HR TEM images of GCT2 sample; (**(b)-1**,**(b)-2**): Schematic diagram of crystal plane spacing of $Li_2Si_2O_5$ and $LiAlSi_4O_{10}$ crystal.

3.5. SEM

The FESEM images of T1~T5 glass-ceramics, as shown in Figure 8, indicate that the grain size is in the range of 60~150mm, and most of them show spherical shape. There are also very few grains with rod-shaped crystals, and the rod-shaped crystals and spherical crystals are non-uniformly distributed. The grain size of T2, T1, T3, T4, and T5 glass-ceramics samples increases sequentially, and the grains in T1, T3, and T4 samples are nearly spherical, with sparse arrangement of grains and intervals of about 10–20 nm. The grains in the T2 sample are fine, with a size of about 60~80 nm, and the highest degree of crystallization with dense arrangement between the grains.

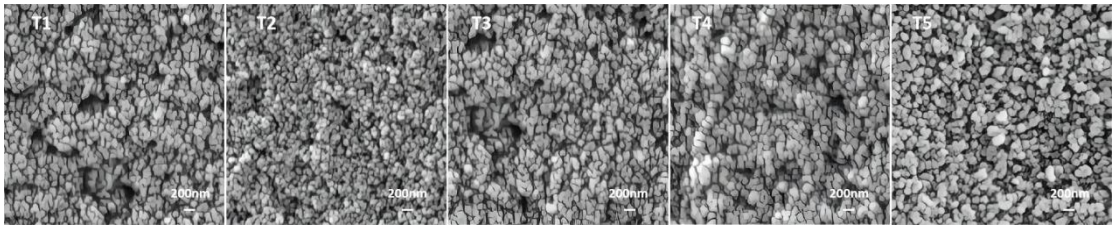

Figure 8. FESEM images of T1~T5 lithium aluminosilicate glass-ceramics.

3.6. Mechanical Properties and Light Transmittance

The bending strength and microhardness of the T1~T5 glass-ceramics are depicted in Figure 9a. The graph demonstrates that the microhardness and bending strength of samples T2, T1, T3, T4, and T5 are decreasing sequentially. The presence of $Li_2Si_2O_5$ and $LiAlSi_4O_{10}$ crystalline phases in the precipitation greatly enhances the microhardness of the glass-ceramics, with the microhardness of the glass-ceramics being determined by their crystallinity and crystal size. The FESEM and XRD results of lithium aluminosilicate glass-ceramics in this paper show that the crystallinity of T2, T1, T3, T4, and T5 decreases in order, while the grain size increases in order, and the microhardness obtained from the test decreases in order. The bending strength of the samples increases as the crystallinity increases and the grain size decreases, as seen in Figure 9a. The finer the grains, the more pronounced the effect of the grains on the glass matrix, which has a higher bending strength and fills in small defects such as microcracks.

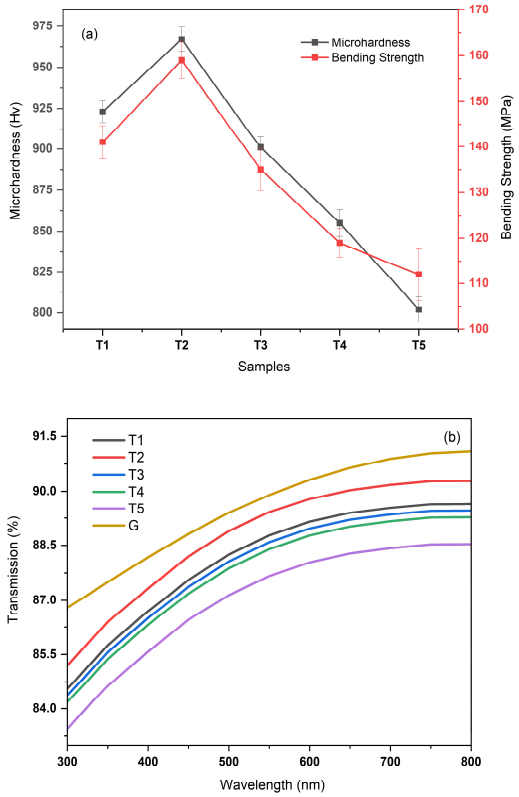

Figure 9. (**a**) Schematic of the flexural strength and microhardness of T1~T5 glass-ceramics; (**b**) visible-light transmission curve of glass-ceramics.

Figure 9b shows the transmittance curves of T1~T5 and base-glass; compared with the base-glass, the visible-light transmission of the five glass-ceramics samples decreased. The transmittance of the T5 sample in the NIR band (600~800 nm) is the lowest, about 88.9%, indicating that the T5 sample has the largest grain size and the strongest scattering effect, which affects the transmittance. As mentioned earlier, the glass-ceramics must meet certain conditions to be transparent, one being that the grain size in the glass matrix is small enough so that the incident light will not be scattered when it is injected into the glass-ceramics; the second is that the precipitated crystals have a refractive index very close to that of the base-glass, i.e., the refractive index matches. It can be seen that the T5 glass-ceramics can maintain high transparency because the precipitated crystals are nanocrystals of small enough size, and the refractive indices of the two main $Li_2Si_2O_5$ and $LiAlSi_4O_{10}$ crystals do not differ from that of the residual glass phase by more than 0.05%, which can be regarded as matching the refractive indices of the crystalline phase and the glass phase.

4. Conclusions

In this paper, the effect of composition on the microstructure and dielectric properties of lithium aluminosilicate glass-ceramics was investigated by adjusting the Li/Na molar ratio. The five lithium aluminosilicate base-glasses were heat-treated separately. Combined with XRD and TEM analysis, $Li_2Si_2O_5$ and $LiAlSi_4O_{10}$ crystals were precipitated from T1 to T5 lithium aluminosilicate glasses, but the crystallinity and crystal ratios were different. Among them, the crystallinity of glass-ceramics T2, T1, T3, T4, and T5 decreased in order. With the precipitation of $Li_2Si_2O_5$ and $LiAlSi_4O_{10}$, the dielectric constants of the T1~T5 glass-ceramics decreased subsequently due to their lower dielectric constants than base-glasses. The presence of crystals in the glass matrix solidified the alkali metal ions, making it difficult for them to move under the electric field. Therefore, the dielectric loss values of T1~T5 glass-ceramics decreased as the amount of precipitated crystals increased.

From the FESEM images and XRD test results, it could be seen that the grain size of lithium aluminosilicate glass-ceramics T2, T1, T3, T4, and T5 increased in order, while the crystallinity decreased in order, and their flexural strength and microhardness also showed a change pattern from high to low. In terms of transmittance, since the refractive indices of $Li_2Si_2O_5$ and $LiAlSi_4O_{10}$ crystals were very close to that of the base-glass, the grain size becomes the most important factor affecting the optical properties. The T2 glass-ceramics had the highest transmittance in the near-infrared light band (600–800 nm), over 90%. This glass-ceramics had optical properties close to those of existing cover glass and became a better choice for 5G communication devices due to better mechanical properties and lower dielectric loss.

Author Contributions: Methodology, Y.M.; data curation, L.K. and W.W.; writing—original draft, M.L.; funding acquisition, H.J. All authors have read and agreed to the published version of the manuscript.

Funding: This work was supported by National Natural Science Foundation of China (U22A20124), Key Scientific & Technological Project of Hainan Province (ZDKJ2021049), Collaborative innovation project (XTCX2022HYC26).

Data Availability Statement: The data presented in this study are available in the article.

Acknowledgments: We acknowledge Fanhou Kong (Shandong Institute of Petroleum and Chemical Technology) for providing language help.

Conflicts of Interest: The authors declare no conflict of interest.

References

1. Liu, S.; Wang, J.; Ding, J.; Hao, H.; Zhao, L.; Xia, S. Crystallization, microstructure and dielectric properties of the SrO-BaO-Nb_2O_5-Al_2O_3-SiO_2 based glass ceramics added with ZrO_2. *Ceram. Int.* **2019**, *45*, 4003–4008. [CrossRef]
2. Yoon, S.O.; Shim, S.H.; Kim, K.S.; Park, J.G.; Kim, S. Low-temperature preparation and microwave dielectric properties of ZBS glass–Al_2O_3 composites. *Ceram. Int.* **2009**, *35*, 1271–1275. [CrossRef]
3. Chen, J.; Huanping, W.; Siqiao, F. Effects of $CaSiO_3$ addition on sintering behavior and microwave dielectric properties of Al_2O_3 ceramics. *Ceram. Int.* **2011**, *37*, 989–993. [CrossRef]
4. Fang, Y.; Li, L.; Xiao, Q.; Chen, X.M. Preparation and microwave dielectric properties of cristobalite ceramics. *Ceram. Int.* **2012**, *38*, 4511–4515. [CrossRef]
5. Chen, G.; Liu, X. Sintering, crystallization and properties of MgO-Al_2O_3-SiO_2 system glass-ceramics containing ZnO. *J. Alloy. Compd.* **2007**, *431*, 282–286. [CrossRef]
6. Sohn, S.; Choi, S. Crystallization behavior in the glass system MgO-Al_2O_3-SiO_2: Influence of CeO_2 addition. *J. Non-Cryst. Solids* **2001**, *282*, 221–227. [CrossRef]
7. Imanaka, Y. *Multilayered Low Temperature Cofired Ceramics (LTCC) Technology*; Springer Science + Business Media: New York, NY, USA, 2005.
8. Zanotto, E.D. A bright future for glass-ceramics. *Am. Ceram. Soc. Bull. Am. Ceram. Soc.* **2010**, *89*, 19–27.
9. Rödel, J.; Kounga, A.B.N.; Weissenberger-Eibl, M.; Koch, D.; Bierwisch, A.; Rossner, W.; Hoffmann, M.J.; Danzer, R.; Schneider, G. Development of a roadmap for advanced ceramics: 2010–2025. *J. Eur. Ceram. Soc.* **2009**, *29*, 1549–1560. [CrossRef]
10. Arnault, L.; Rivière, A. Relaxation mechanisms and microstructure in glass and glass-ceramics. *J. Alloys Compd.* **2000**, *310*, 32–35. [CrossRef]
11. Chen, G.; Ma, M.; Wei, A.; Liu, Z.; Zhang, F.; Mitchell, A.; Li, Y. The dielectric, thermal properties and crystallization mechanism of Li–Al—B–Si—O glass—Ceramic systems as a new ULTCC material. *Ceram. Int.* **2019**, *45*, 19689–19694. [CrossRef]
12. Qing, Z. The effects of B_2O_3 on the microstructure and properties of lithium aluminosilicate glass-ceramics for LTCC applications. *Mater. Lett.* **2018**, *212*, 126–129. [CrossRef]
13. Krasnikov, A.S.; Berezhnoi, A.I.; Krasnikova, M.D. Effect of ions with different radii on the properties of lithium aluminosilicate photosensitive devitrified glasses. *Glass Ceram.* **1998**, *55*, 106–110. [CrossRef]
14. Savabieh, H.; Alizadeh, P.; Dasilva, Y.A.R.; Erni, R.; Clemens, F.J. Investigation of dielectric properties and microstructure of sintered 13·2Li_2O-67·6SiO_2-14·49Al_2O_3-3·3TiO_2-0.4BaO-0.97ZnO glass-ceramics. *J. Eur. Ceram. Soc.* **2017**, *37*, 631–639. [CrossRef]
15. Zhou, Z.Q.; He, F.; Shi, M.J.; Xie, J.; Wan, P.; Cao, D.H. Effect of Na_2O Content on the Structure and Properties of LAS Glass-ceramics Prepared by Spodumene. *J. Wuhan Univ. Technol.-Mat. Sci. Edit.* **2022**, *37*, 794–800. [CrossRef]
16. Shi, J.; He, F.; Xie, J.; Liu, X.; Yang, H. Effects of Na_2O/BaO ratio on the structure and the physical properties of low-temperature glass-ceramic vitrified bonds. *Ceram. Int.* **2018**, *44*, 10871–10877. [CrossRef]
17. Zhang, W.T.; He, F.; Xiao, Y.; Xie, M.Q.; Xie, J.L.; Sun, R.J.; Yang, H.; Luo, Z.H. Effects of Al/Na and Heat Treatment on the Structure and Properties of Glass Ceramics from Molten Blast Furnace Slag. *Ceram. Int.* **2019**, *45*, 13692–13700. [CrossRef]

18. Li, W.C.; Wang, X.; Chen, H.Y.; Zhang, X.F.; Hu, L.L.; Chen, S.B. Influence of fluorine content on crystallization and mechanical properties of SiO_2-Li_2O glass-ceramics. *Ceram. Int.* **2023**, *49*, 29123–29132. [CrossRef]
19. Ji, C.J.; Li, L.Y.; Gao, W.K.; Wang, J.; Han, J.J. Influence of Al_2O_3/SiO_2 ratio in multicomponent LNAS glasses and glass-ceramics on the crystallization behavior, microstructure and mechanical performance. *Ceram. Int.* **2023**, *49*, 10652–10662. [CrossRef]
20. Chen, M.; He, F.; Shi, J.; Xie, J.; Yang, H.; Wan, P. Low Li_2O content study in Li_2O-Al_2O_3-SiO_2 glass-ceramics. *J. Eur. Ceram. Soc.* **2019**, *39*, 4988–4995. [CrossRef]
21. Kucharczyk, S.; Sitarz, M.; Zajac, M.; Deja, J. The effect of CaO/SiO_2 molar ratio of CaO-Al_2O_3-SiO_2 glasses on their structure and reactivity in alkali activated system. *Spectrochim. Acta Part A Mol. Biomol. Spectrosc.* **2018**, *194*, 163–171. [CrossRef]
22. Partyka, J.; Sitarz, M.; Leśniak, M.; Gasek, K.; Jeleń, P. The effect of SiO_2/Al_2O_3 ratio on the structure and microstructure of the glazes from SiO_2–Al_2O_3–CaO–MgO–Na_2O–K_2O system. *Spectrochim. Acta Part A Mol. Biomol. Spectrosc.* **2015**, *134*, 621–630. [CrossRef]
23. Li, H.; Su, Y.; Li, L.Y.; Strachan, D.M. Raman spectroscopic study of gadolinium(III) in sodium-aluminoborosilicate glasses. *J. Non. Cryst. Solids* **2001**, *292*, 167–176. [CrossRef]
24. Doweidar, H.; El-Damrawi, G.; Al-Zaibani, M. Distribution of species in Na2O–CaO–B2O3 glasses as probed by FTIR. *Vib. Spectrosc.* **2013**, *68*, 91–95. [CrossRef]
25. Shi, J.; He, F.; Ye, C.; Hu, L.; Xie, J.; Yang, H.; Liu, X. Preparation and characterization of CaO–Al_2O_3–SiO_2 glass-ceramics from molybdenum tailings. *Mater. Chem. Phys.* **2017**, *197*, 57–64. [CrossRef]
26. Reddy, A.A.; Goel, A.; Tulyaganov, D.U.; Kapoor, S.; Pradeesh, K.; Pascual, M.J.; Ferreira, J.M.F. Study of calcium–magnesium–aluminum–silicate (CMAS) glass and glass-ceramic sealant for solid oxide fuel cells. *J. Power Sources* **2013**, *231*, 203–212. [CrossRef]
27. Mukherjee, D.P.; Das, S.K. The influence of TiO_2 content on the properties of glass ceramics: Crystallization, microstructure and hardness. *Ceram. Int.* **2014**, *40*, 4127–4134. [CrossRef]
28. Arvind, A.; Kumar, R.; Deo, M.N.; Shrikhande, V.K.; Kothiyal, G.P. Preparation, structural and thermo-mechanical properties of lithium aluminum silicate glass–ceramics. *Ceram. Int.* **2009**, *35*, 1661–1666. [CrossRef]
29. Li, Y.; Liang, K.; Cao, J.; Xu, B. Spectroscopy and structural state of V^{4+} ions in lithium aluminosilicate glass and glass–ceramics. *J. Non. Cryst. Solids* **2010**, *356*, 502–508. [CrossRef]
30. Naskar, M.K.; Chatterjee, M. A novel process for the synthesis of lithium aluminum silicate powders from rice husk ash and other water-based precursor materials. *Mater. Lett.* **2005**, *59*, 998–1003. [CrossRef]
31. Nevolina, L.A.; Shtenberg, M.V.; Zherebtsov, D.A.; Koroleva, O.N. Structure and crystallizability of K_2O-B_2O_3-SiO_2 and K_2O-B_2O_3-GeO_2 glasses: Effect of composition and heat treatment mode. *Ceram. Int.* **2023**. [CrossRef]
32. Li, M.H.; Dong, C.; Ma, Y.P.; Jiang, H. Light-Transmitting Lithium Aluminosilicate Glass-Ceramics with Excellent Mechanical Properties Based on Cluster Model Design. *Nanomaterials* **2023**, *13*, 530. [CrossRef]
33. Vomacka, P.; Babushkin, O.; Warren, R. Zirconia as a nucleating agent in a yttria-alumina-silica glass. *J. Eur. Ceram. Soc.* **1995**, *15*, 1111–1117. [CrossRef]
34. Du, J.; Jones, B.; Lanagan, M. Preparation and characterization of dielectric glass-ceramics in Na_2O–PbO–Nb_2O_5–SiO_2 system. *Mater. Lett.* **2005**, *59*, 2821–2826. [CrossRef]
35. Chakrabarti, A.; Molla, A.R. $BaBi_2Ta_2O_9$ based glass-ceramics: Influence of ZrO_2 on crystallization kinetics, microstructure and dielectric properties. *J. Alloy. Compd.* **2019**, *805*, 247–257. [CrossRef]